Research on Embedded Integration of Robot Power System and Control Module: A Disinfection Robot Control System Based on an ARM Controller

Weixi Huang[1*], Wenwei Li[2], Yongqian Xu[1], Jia'nan Liang[1]

[1] South China Robotics Innovation Research Institute, Foshan, 528300, China

[2] Foshan Zhiyouren Technology Co., Ltd., Foshan, 528300, China

* wxhuang2012@126.com

https://doi.org/10.70695/IAAI202504A9

Abstract

Currently, the power system and control module of disinfection robots have low coupling, resulting in shortcomings in energy efficiency and reliability. Therefore, this paper proposes an embedded integrated control system based on an ARM controller. First, system-level indicators such as overall weight, battery life, speed, and dosage are given, and a unified DC bus and multi-level DC/DC topology are designed. Then, a power-control integrated hardware architecture and an RTOS real-time software platform are formed to achieve coordination between motion control, power management, and disinfection execution. Furthermore, a differential motion control algorithm and a dosage constraint strategy are designed. Experimental results show that the system has high power efficiency, relatively stable temperature rise, small trajectory tracking error, speed response that meets real-time requirements, uniform disinfection coverage, and a high logarithmic kill rate under various operating conditions. Its robustness is verified after long-term operation and fault injection tests.

Keywords Disinfection Robot; Embedded Control; Power System; ARM Controller; Trajectory Tracking; Reliability

1 Introduction

In recent years, the demand for efficient and stable environmental disinfection in public places has risen rapidly, driving the growth of mobile disinfection robot applications. The existing research can be summarized in time as follows: Hassan et al. proposed a hybrid prototype, focusing on multi-mode collaboration to improve coverage efficiency [1]; Bratu et al. designed an autonomous UV-C robot, focusing on UV disinfection efficiency and its dual safety mechanism [2]; Ma et al. developed a modular UVC platform, but there is still some separation in power and control [3]; Cao et al. used a dual-function robot with safety filtering to complete the collaborative work of path and protection, but this collaboration relies on complex perception fusion [4]; Chio et al. used disinfection modeling to improve the uniformity of navigation, but the system integration is not sufficient [5]; Zaman et al. gave a low-cost solution, but its energy efficiency and power capability are lacking [6]; Byun et al. investigated the effectiveness of combining UV-C with wiping in hospitals, but did not pay enough attention to energy allocation under high load [7]; In addition, Sulistiyowati et al. proposed an IoT spraying robot [8]; Krejčí et al. studied the embedded structure in IoT robots [9]; Vrochidou et al. demonstrated how embedded fusion can enhance reliability in agricultural robots [10]. Current research has made some progress in disinfection methods and safety guidance, but it is still constrained by factors such as insufficient power-control coupling, low energy efficiency and poor immediacy. Therefore, it is necessary to build a deep embedded fusion architecture with ARM as the core to improve energy efficiency, response speed and safety. This paper proposes a highly integrated control system suitable for indoor use, creates a unified power-control framework, and formulates disinfection strategies from multiple sources. After experimental verification, the energy efficiency, control accuracy and disinfection performance of the system have been improved.

2 System Requirements Analysis and Overall Architecture

2.1 Definition of Power and Control Requirements

Indoor disinfection tasks impose limitations on robot quality, battery life, and mobility, requiring the use of limited battery capacity to ensure a stable disinfectant dosage and achieve a certain coverage rate. During this process, the system design phase must clearly define indicators such as overall robot weight, rated operating time, maximum operating speed, maximum gradient, and minimum disinfectant dosage per unit area, and these system-level constraints should be presented in Table 1 in the form of "target value/acceptance limit".

Table 1. System-level design targets

Parameter	Symbol	Target Value	Acceptance Limit	Description
Robot mass	m	≤ 60 kg	≤ 65 kg	Including battery and disinfectant
Endurance time	t_{req}	2.0 h	1.5 h	Continuous disinfection
Rated electrical power	P_{rated}	300 W	280 W	Nominal cruise
Peak Electrical Power	P_{peak}	600 W	550 W	Acc./slope
Maximum linear speed	$v_{\max}$	1.0 m/s	0.8 m/s	Corridor operation
Maximum slope	$\theta_{\max}$	8°	6°	Ramp capability
Minimum disinfectant dose	$D_{\min}$	10 mL/m²	9 mL/m²	Per pass
Coverage ratio	—	≥ 95%	≥ 90%	Within target area
Allowable DC bus voltage sag	$\Delta U / U$	≤ 10%	≤ 15%	Under peak load

On the power side, the rated power of each subsystem and the mission endurance determine the lower limit of the battery capacity. Considering the nominal DC bus voltage U_{nom} and the overall system efficiency η_{sys}, the battery capacity is estimated according to equation (1) to guide cell selection and series/parallel configuration:

$$C_{bat} = \frac{\sum_i P_i t_{req}}{U_{nom} \eta_{sys}} \tag{1}$$

Where, C_{bat} is the nominal capacity of the battery (Ah), P_i and is the i-th ... The rated power of each subsystem (W) t_{req} is the target range (h), U_{nom} the nominal voltage of the DC bus (V) η_{sys} is the overall efficiency of the machine (dimensionless).

2.2 Overall Structure and Functional Breakdown of the Disinfection Robot

The system adopts a unified DC bus and modular electromechanical architecture. The chassis implements differential drive, the disinfection module includes spray and UVC functions, the sensing module integrates LiDAR, depth camera and IMU, the communication module connects to the host computer and cloud, and the ARM module is responsible for control and scheduling. The interfaces of each unit are standardized, which facilitates maintenance and expansion. Figure 1 uses a three-layer block diagram to show the signal and power flow between the chassis, drive, disinfection, sensing, HMI, wireless and controller.

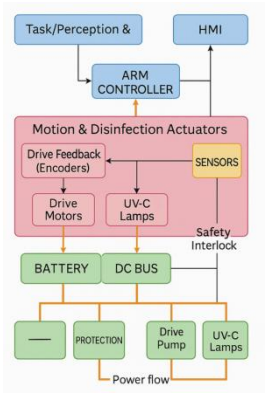

Fig. 1. Overall mechatronic architecture of the disinfection robot

Bus power balancing is modeled according to equation (2), which equates the power demand of each subsystem to the DC bus side, and is used to verify the power supply margin under different operating conditions:

$$P_{bus} = \sum_{i} \frac{U_i I_i}{\eta_{conv}} \tag{2}$$

Where, is P_{bus} the total power on the DC bus side (W), U_i and is the i-th ... The operating voltage (V) of each subsystem I_i is the i -th subsystem. The operating current (A) η_{conv} of each subsystem is the corresponding power conversion unit efficiency (dimensionless).

2.3 ARM-based Power-control Embedded Integrated Architecture

As shown in Figure 2, the system integrates the power and control modules on a multi-layer board, and uses partitioning and isolation devices to achieve high and low voltage isolation; the 48V battery generates 24V, 12V, and 5V through the main DC/DC converter and multiple Buck/Boost converters, which respectively power the load and control and sensing units. The ARM completes drive communication, power modulation, and status acquisition through CAN, PWM, and ADC/SPI/I²C; emergency stop, overcurrent, and overtemperature are forcibly disconnected from the power path by independent hardware links. The duty cycle of the main buck topology and the relationship between the input and output voltage are shown in equation (3):

$$D = \frac{U_{out}}{U_{in}} \tag{3}$$

Among them, D is the duty cycle of the main switching device (dimensionless), U_{in} is the input voltage, i.e., the battery or the DC bus voltage of the previous stage (V), and is the U_{out} target voltage on the output side (V).

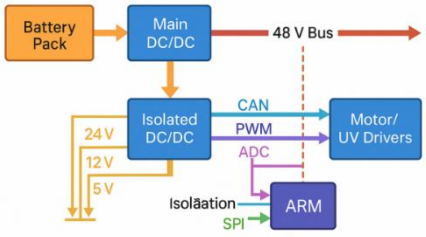

Fig. 2. Embedded power–control integration topology based on ARM

3 Design and Implementation of Embedded Power System and Control Module

3.1 Design of DC Bus and Power Conversion Unit

The DC bus voltage needs to be balanced between efficiency, loss, and withstand voltage. This system uses 48V as the main bus to drive the motor and UVC unit, and generates 24V, 12V, and 5V from the main DC/DC converter and multiple Buck/Boost converters to supply various loads. The main DC/DC converter is rated at 500W, and its efficiency is optimized at approximately 70% load point to ensure cruise cooling margin. The efficiency and loss of the conversion stage are modeled according to Equation (4), and the loss distribution is obtained through [variable] P_{in} , P_{out} which is used for the design of heat sink and copper foil width.

$$\eta_{conv} = \frac{P_{out}}{P_{in}}, \quad P_{loss} = P_{in} - P_{out} \tag{4}$$

Where η_{conv} is the power conversion efficiency (dimensionless), P_{out} is the output power (W), P_{in} is the input power (W), P_{loss} and is the power loss (W). The bus ripple is estimated by equation (5) and used to determine the nominal capacity and ripple current level of the output filter capacitor to meet the voltage ripple constraints of sensitive loads.

$$\Delta U_{\text{ripple}} \approx \frac{I_{load}}{C_{out} f_{sw}} \tag{5}$$

Here ΔU_{ripple} , the bus voltage ripple amplitude (V), I_{load} the load current (A), C_{out} the output side filter capacitor (F), f_{sw} and the switching frequency (Hz) are given.

3.2 ARM Control Module Hardware and Real-Time Software Platform

The control module uses an ARM Cortex-M microcontroller of approximately 200 MHz, which has a built-in FPU and integrates various types of ADCs, PWM, CAN, Ethernet, and UART/SPI/I²C interfaces. By using voltage division, current sampling, and isolation amplification, the reliability of measurements in high-noise environments can be improved. The software relies on a lightweight RTOS to schedule core tasks such as motion, power, disinfection, human-machine interaction, and communication. The duration and load of the tasks are shown in Table 2. There are also some critical interrupts involving encoders, faults, and emergency stop inputs, thus achieving the goal of rapid response to abnormal conditions.

Table 2. Task set and CPU load of ARM controller

Task name	Period / ms	Avg.exec.time / μs	CPU load / %	Priority (0 = lowest)
Motion control	5	80	8	4
Power Management	10	60	4	3
Disinfection control	20	70	3.5	3
Sensor Fusion	20	120	6	2
HMI & diagnostics	100	150	1.5	1
Communication stack	10	100	5	2
Background/maintenance	1000	200	< 1	0

3.3 Implementation of Motion Control Algorithm and Drive Interface

The chassis adopts a differential drive structure. The left and right drive wheels are driven by independent motors. There is a specific relationship between the linear velocity (v) and angular velocity and (ω) the wheel speed (r) . This relationship can be expressed by equation (6). The controller calculates the expected angular velocity of the left and right wheels according to the value specified by the planning layer (v,ω) , and then achieves the following target through closed-loop control.

$$\begin{bmatrix} v \\ \omega \end{bmatrix} = \begin{bmatrix} \frac{r}{2} & \frac{r}{2} \\ \frac{r}{L} & -\frac{r}{L} \end{bmatrix} \begin{bmatrix} \omega_L \\ \omega_R \end{bmatrix} \tag{6}$$

Where is v the robot linear velocity (m/s), ω is the robot angular velocity (rad/s), r is the radius of the drive wheel (m), L is the center distance between the two drive wheels (m), ω_L、 ω_R and are the angular velocities of the left and right wheels (rad/s), respectively. Speed control employs a discrete PID algorithm to achieve precise adjustment of wheel speed. Equation (7) gives the discrete form of the control law, and the error $e(k)$ is obtained from the difference between the desired speed and the actual speed:

$$u(k) = K_p e(k) + K_i \sum_{j=0}^{k} e(j) T_s + K_d \frac{e(k) - e(k-1)}{T_s} \tag{7}$$

Here, $u(k)$ represents the control output at the i-th k sampling moment, and its unit is a dimensionless quantity, such as the PWM duty cycle; $e(k)$ represents the current speed error (unit: m/s); $e(k-1)$ represents the speed error during the previous sampling period (unit: m/s); K_p, K_i, K_d represents the proportional, integral, and derivative coefficients respectively (must meet the corresponding unit requirements); and T_s refers to the sampling duration (unit: s). The speed loop runs with a 5-millisecond delay. The PID parameters are tuned through simulation and experiments to balance bandwidth and steady-state accuracy. The PWM is output to the driver by the timer. The driver has an internal current loop and an external speed loop, forming a nested control architecture.

3.4 Disinfection Process Control Strategies and Safety Interlocks

In spraying mode, the dose per unit area is determined by the flow rate, spraying duration, and coverage area; the control strategy adjusts the pump speed or valve duty cycle in real time according to the vehicle speed to keep the dose within the target range under different paths and speeds; the dose model is shown in equation (8), which is used to calculate the flow rate from the target dose and correct it online as the vehicle speed changes:

$$D = \frac{C \cdot Q \cdot t}{A} \tag{8}$$

Where, D is the disinfectant dosage per unit area (mL/m²), C is the disinfectant concentration (dimensionless or %), Q is the volumetric flow rate (mL/s), t is the spraying time (s), A and is the coverage area (m²). For safety, the system imposes inequality constraints on variables such as dosage, speed, and obstacle distance, as shown in equation (9):

$$D_{\min} \le D \le D_{\max}, \quad v \le v_{\max}, \quad d_{\text{obstacle}} \ge d_{\text{safe}} \tag{9}$$

Here, $D_{\min}$ and $D_{\max}$ represent the lower and upper limits of the dosage (in mL/m²), respectively; v represents the current vehicle speed (in m/s); $v_{\max}$ is the maximum permissible vehicle speed (in m/s); d_{obstacle} is the distance from the robot to the nearest obstacle (in m); and d_{safe} is the safety distance

threshold (in m). Human body detection, emergency stop, and liquid level monitoring are accessed via hardware interlocks and dual software channels. If any condition becomes abnormal, the disinfection unit will stop and a braking operation will be performed. The safety threshold, after calibration, is stored in non-volatile memory and is checked by power and safety task duration.

4 Experimental Platform Setup and Performance Testing

4.1 Experimental Platform and Operating Condition Design

The experimental platform was constructed based on the prototype mentioned earlier. Its chassis, power module, and ARM controller remained unchanged; only a replaceable disinfection module bracket and sensor mounting positions were added. The test site included marked lines in the corridors, lobby, and ward passageways, creating obstacle simulation scenarios. Operating conditions were determined by a composite of speed, load, and initial SoC, covering various states from light load with high power to heavy load with low power. These states were numbered according to Tab.3 and managed uniformly. During testing, the system simultaneously recorded voltage, current, temperature, and position information, providing data support for subsequent power, trajectory, and disinfection performance analysis.

Table 3. Test scenarios and operating conditions

Scenario ID	Area type	Area / m²	Obstacles (#)	Target speed / m·s⁻¹	Disinfection mode	Initial SoC / %
S1	Straight corridor	80	4	0.5	Spray	95
S2	Straight corridor	80	8	0.8	UV-C	90
S3	Open hall	200	6	0.6	Spray + UV-C	85
S4	Open hall	200	10	1.0	Spray	80
S5	Ward corridor	60	12	0.4	UV-C	75
S6	Ward corridor	60	16	0.6	Spray + UV-C	70

4.2 Power System Efficiency and Range Performance Testing

For power and battery life testing, select representative modes such as standby, low/high speed cruise, acceleration, full load disinfection, and ramp. Use a programmable load and power analyzer to record bus voltage, current, and main DC/DC power. Use thermocouples to detect device temperature rise. In each mode, the device must be allowed to run stably for at least 15 minutes, and the battery SoC must be within the specified range before switching.

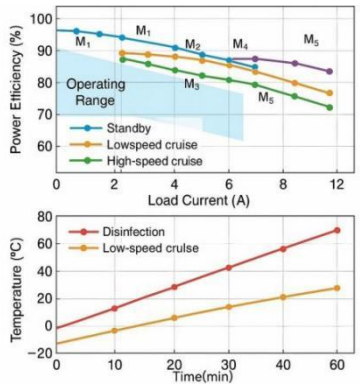

Fig. 3. Power efficiency and temperature vs load current

Fig.3 shows that the system maintains high efficiency at 40%–70% of rated current. Although the efficiency drops slightly under full load and ramp conditions, it is still higher than the 90% lower limit in Tab. 4. The figure below shows that the temperature rise of the MOSFET and inductor stabilizes under

long-term full load and does not trigger protection. Tab. 4 summarizes the power, efficiency and range of each mode, providing a basis for task power budgeting and charging strategies.

Table 4. Power efficiency and runtime in different modes

Mode ID	Description	Avg. current / A	Avg. power / W	Efficiency / %	Est.runtime / h	Maxcase temp /°C
M1	Standby	1.2	55	92	3.8	38
M2	Low-speed cruise	4.5	210	94	2.4	52
M3	High-speed cruise	6.8	320	93	1.9	57
M4	Acceleration bursts	9.5	450	91	1.6	63
M5	Full-load disinfection	7.8	360	92	1.8	59
M6	Ramp climbing	8.6	400	90	1.7	61

4.3 Motion Control Accuracy and Real-time Performance Experiment

The differential chassis trajectory tracking and real-time control experiment selected straight, circular, S-shaped paths and complex paths including doorway passage and sharp turns. The host computer generated reference trajectories offline. The robot ran according to the scenario described in section 4.1. Each trajectory needed to be repeated 10 times. The actual trajectory was obtained by combining a laser rangefinder and an odometer. The ARM controller recorded the speed commands, speed feedback and timestamps during the control period.

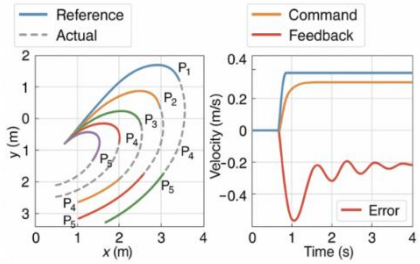

Fig. 4. Trajectory tracking and velocity response

Fig.4 shows the superimposed expected and measured trajectories on the left to observe the error distribution under different paths; the right figure shows the command, feedback and instantaneous errors in the speed step to evaluate acceleration and deceleration stability; Tab. 5 summarizes the RMS error, maximum lateral error and average delay of each path. The results show that the errors of straight lines and circular arcs are small, and although the composite path has a peak at sharp bends, it still meets the index.

Table 5. Trajectory tracking and control latency metrics

Path ID	Path type	RMS error / cm	Max lateral error / cm	Avg. control delay / ms	Overshoot in speed / %	Path length deviation / %
P1	Straight	1.2	3.0	2.1	3	0.5
P2	Circular (R=2 m)	1.8	4.5	2.4	4	0.8
P3	S-curve	2.6	6.2	2.7	5	1.3
P4	Doorway crossing	2.1	5.5	2.9	4	1.0
P5	Tight turn (90°)	3.4	7.8	3.1	6	1.9
P6	Mixed corridor	2.9	6.9	3.0	5	1.6

4.4 Disinfection Effectiveness Evaluation and Coverage Uniformity Analysis

The disinfection effectiveness was evaluated using a combined method of bacterial culture dishes and chemical indicator cards. Based on the scenarios in Table 3, culture dishes or indicator cards were placed in a grid layout on the corridor floor and walls. These dishes or cards corresponded to different path planning and velocity-flow parameter synthesis scenarios. Before the experiment, samples underwent standardized contamination treatment. After one or more disinfection cycles performed by the robot, the samples were incubated in a constant temperature incubator, and then the colony count was calculated or the color change of the indicator cards was read. Each strategy was repeated at least five times to reduce random errors.

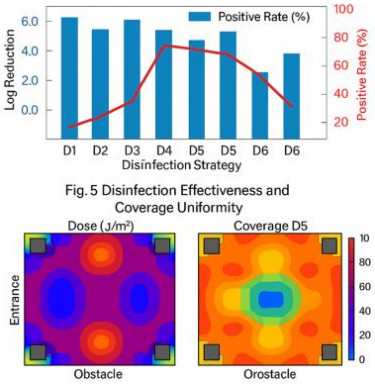

Fig. 5. Disinfection effectiveness and coverage uniformity

Fig.5 shows the logarithmic kill rate and positivity rate under different strategies using parallel bars, clearly demonstrating the difference in effectiveness between single-pass and double-cross-pass strategies. The bottom figure presents the dose distribution using a 0.5 m × 0.5 m thermal grid, with darker colors indicating more adequate coverage. Tab. 6 summarizes the kill rate, positivity rate, and uniformity of the six strategies, showing that under dose-limited conditions, bidirectional cross-pass and adaptive speed significantly improve coverage uniformity and reduce dead zones and overspray.

Table 6. Disinfection performance under different coverage strategies

Strategy ID	Path & control strategy	Avg. log reduction	Positive rate / %	Uniformity index (0–1)	Over-dose area / %	Under-dose area / %
D1	Single pass, constant speed	3.1	12	0.78	18	9
D2	Dual pass, orthogonal	3.8	5	0.86	15	4
D3	Edge-following	3.4	9	0.81	20	7
D4	Spiral in open hall	3.6	7	0.84	17	6
D5	Adaptive speed vs. dose	3.9	4	0.89	13	3
D6	Non-uniform test pattern	2.7	18	0.69	twenty four	13

4.5 System Reliability and Robustness Verification

The reliability test consists of two parts: long-term continuous operation and fault injection. In the continuous operation test, the robot alternates between scenarios S2 and S5 to perform disinfection tasks for more than 8 hours, collecting data on the changes in battery SoC, DC bus voltage, and power module temperature over time. During the fault injection test, situations such as artificially applied voltage drops, partial sensor blockage, and network interference are introduced. The system's protection actions, the time from the occurrence of a problem to recovery, and the task completion status are recorded.

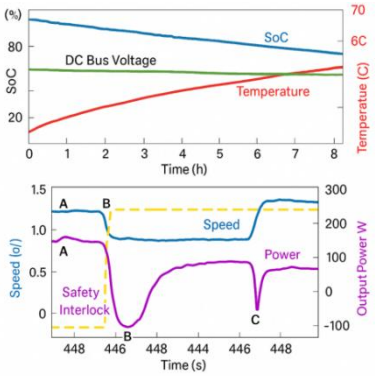

Fig. 6. Long-term operation results and fault response

Fig.6 shows the SoC drop, slight bus voltage fluctuation, and slow temperature stabilization during long-term operation, verifying the stability of power and thermal management. The figure below compares the speed, power, and safety interlock status before and after fault injection, indicating that the system can limit power or stop in an emergency when the voltage drops and sensors are blocked, and resume operation on time after the conditions are restored.

5 Conclusions and Outlook

This paper takes an indoor mobile disinfection robot as the research object and creates an embedded architecture that deeply integrates the power system and control module. This architecture includes system requirements, hardware topology, and control software implementation, thus forming a relatively complete planning process. Utilizing a unified DC bus and an ARM integrated control platform, the drive, power supply operation, and disinfection execution units achieve collaborative cooperation in electrical interfaces and real-time scheduling, comprehensively considering efficiency, size, and safety factors. A combination of high-speed motion control and dose constraint strategies ensures trajectory accuracy and disinfection uniformity. Experimental results show that under typical operating conditions, the system has high power efficiency, acceptable temperature rise, and motion control errors at the centimeter level. The disinfection coverage and logarithmic kill rate meet the design specifications. After long-term operation and fault injection tests, the system's reliability and robustness are further confirmed, providing a feasible reference example for the design of highly integrated control systems for similar service robots.

Acknowledgement

This work was supported by Foshan Science and Technology Innovation Project under Grant FS0AA-KJ919-4402-0060; Core Technologies Research Project of Shunde District under Grant 2130218003022.

Conflicts of Interest

The authors declare no conflicts of interest.

References

1. Hassan, M. M., Amin, A., Rahman, M. M., et al. (2024). Hybrid disinfection robot: A prototype. In 2024 IEEE Region 10 Symposium (TENSYMP) (pp. 1-6). IEEE.
2. Bratu, D. V., Zolya, M. A., & Moraru, S. A. (2024). RoboCoV Cleaner: An indoor autonomous UV-C disinfection robot with advanced dual-safety systems. Sensors, 24(3).
3. Ma, Y., Xi, N., Xue, Y., et al. (2022). Development of a UVC-based disinfection robot. Industrial Robot: The International Journal of Robotics Research and Application, 49(5), 913-923.
4. Cao, Y., Wu, Z., Chen, I. M., et al. (2025). Design of a dual-function autonomous disinfection robot with safety filter-based motion control. Robotics, 14(3), 26.

5. Chio, I., Ruan, K., Wu, Z., et al. (2022). Design and autonomous navigation of a new indoor disinfection robot based on disinfection modeling. IEEE Transactions on Automation Science and Engineering, 20(1), 649-661.
6. Zaman, A., Majib, M. S., Tanjim, S. A., et al. (2022). UVC-PURGE: A novel cost-effective disinfection robot for combating COVID-19 pandemic. IEEE Access, 10, 37613-37634.
7. Byun, J., Byun, J., Kang, J., et al. (2025). Autonomous ultraviolet-C disinfection and wiping robot: Assessment in a hospital environment. IEEE Robotics & Automation Magazine.
8. Sulistiyowati, I., & Muhyiddin, M. I. (2021). Disinfectant spraying robot to prevent the transmission of the COVID-19 virus based on the Internet of Things (IoT). Journal of Electrical Technology UMY, 5(2), 61–67.
9. Krejčí, J., Babiuch, M., Babjak, J., et al. (2022). Implementation of an embedded system into the Internet of Robotic Things. Micromachines, 14(1), 113.
10. Vrochidou, E., Tziridis, K., Nikolaou, A., et al. (2021). An autonomous grape-harvester robot: Integrated system architecture. Electronics, 10(9), 1056.

Biographies

1. **Weixi Huang** Master, Engineer, major and research direction: automation technology, optical intelligent processing and testing equipment technology. He has applied for more than 30 technical patents and published over 10 academic papers;
2. **Wenwei Li** PhD, Senior Engineer, with main majors and research directions in intelligent robotics, CAD/CAE digital simulation, mechanical dynamics, and manufacturing informatization. He has applied for 55 technical patents and published over 30 academic papers;
3. **Yongqian Xu** Master, Senior Engineer, main research direction: automation technology and electromechanical professional field, he has applied for technical patents, published more than 20 academic papers, and obtained more than 20 technical patents;
4. **Jia'nan Liang** PhD, Senior Engineer, main research areas: automation technology, machine vision, and intelligent manufacturing technology. He published over 30 academic papers and applied for over 40 technical patents.

機器人功率系統與控制模塊的嵌入式集成實現研究——基於ARM控制器的消毒機器人控制系統

黃偉溪[1]，李文威[2]，徐永謙[1]，梁佳楠[1]

[1]華南智能機器人創新研究院，佛山，中國，528300

[2]佛山智優人科技有限公司，佛山，中國， 528300

摘要：當前，消毒機器人的功率系統和控制模塊耦合度較低，其能效和可靠性也存在短缺。鑑於此，本文提出一種依託 ARM 控制器的嵌入式一體化控制系統。 首先要給出整機質量，續航，速度以及劑量這些系統級別的指標，並且設計統一的 DC 母線以及多級 DC/DC 拓撲；接着形成功率–控制一體化的硬件架構和 RTOS 實時軟件平臺，達成運動控制，功率管理以及消毒執行之間的協同；還要設計差速運動控制算法以及劑量約束策略。實驗結果顯示，該系統在多種工況下功率效率較高，溫升較爲穩定，軌跡跟蹤誤差小，速度響應符合即時性需求，消毒覆蓋面均勻，對數殺滅率較高，經過長時間運行和故障注入試驗後，其魯棒性得到了驗證。

關鍵詞：消毒機器人；嵌入式控制；功率系統；ARM 控制器；軌跡跟蹤；可靠性

1. 黃偉溪，碩士，工程師，主要專業和研究方向爲自動化技術、光學智能加工與檢測裝備技術，累計申請技術專利30餘件，發表學術論文10餘篇；
2. 李文威，博士，高級工程師，主要專業和研究方向爲智能機器人、 數字化仿真、機械動力學、製造業信息化，累計申請技術專利55件，發表學術論文30餘篇；
3. 徐永謙，碩士，正高級工程師，主要研究方向爲自動化技術及機電專業領域，累計申請技術專利，累計發表學術論文20多篇，獲得技術專利20多件；
4. 梁佳楠，博士，高級工程師，主要研究方向爲自動化技術、機器視覺及智能製造技術，累計發表學術論文30餘篇，申請技術專利40餘件。